nature astronomy

SUPPLEMENTARY INFORMATION

https://doi.org/10.1038/s41550-019-0915-8

In the format provided by the authors and unedited.

A basin-free spherical shape as an outcome of a giant impact on asteroid Hygiea

P. Vernazza[1]*, L. Jorda[1], P. Ševeček[2], M. Brož[2], M. Viikinkoski[3], J. Hanuš[2], B. Carry[4], A. Drouard[1], M. Ferrais[5], M. Marsset[6], F. Marchis[1,7], M. Birlan[8], E. Podlewska-Gaca[9,10], E. Jehin[5], P. Bartczak[9], G. Dudzinski[9], J. Berthier[8], J. Castillo-Rogez[11], F. Cipriani[12], F. Colas[8], F. DeMeo[6], C. Dumas[13], J. Durech[2], R. Fetick[1,14], T. Fusco[1,14], J. Grice[4,15], M. Kaasalainen[3], A. Kryszczynska[9], P. Lamy[1], H. Le Coroller[1], A. Marciniak[9], T. Michalowski[9], P. Michel[4], N. Rambaux[8], T. Santana-Ros[16,17], P. Tanga[4], F. Vachier[8], A. Vigan[1], O. Witasse[12], B. Yang[18], M. Gillon[5], Z. Benkhaldoun[19], R. Szakats[20], R. Hirsch[9], R. Duffard[21], A. Chapman[22] and J. L. Maestre[23]

[1]LAM (Laboratoire d'Astrophysique de Marseille) UMR 7326, Aix Marseille Université, CNRS, Marseille, France. [2]Institute of Astronomy, Charles University, Prague, Czech Republic. [3]Mathematics and Statistics, Tampere University, Tampere, Finland. [4]Laboratoire Lagrange, Université Côte d'Azur, Observatoire de la Côte d'Azur, CNRS, Nice, France. [5]Space Sciences, Technologies and Astrophysics Research Institute, Université de Liège, Liège, Belgium. [6]Department of Earth, Atmospheric and Planetary Sciences, MIT, Cambridge, MA, USA. [7]SETI Institute, Carl Sagan Center, Mountain View, CA, USA. [8]IMCCE, Observatoire de Paris, Paris, France. [9]Astronomical Observatory Institute, Faculty of Physics, Adam Mickiewicz University, Poznań, Poland. [10]Institute of Physics, University of Szczecin, Szczecin, Poland. [11]Jet Propulsion Laboratory, California Institute of Technology, Pasadena, CA, USA. [12]European Space Agency, ESTEC - Scientific Support Office, Noordwijk, the Netherlands. [13]TMT Observatory, Pasadena, CA, USA. [14]ONERA, The French Aerospace Lab, Chatillon, France. [15]School of Physical Sciences, The Open University, Milton Keynes, UK. [16]Departamento de Física, Ingeniería de Sistemas y Teoría de la Señal, Universidad de Alicante, Alicante, Spain. [17]Institut de Ciències del Cosmos, Universitat de Barcelona, Barcelona, Spain. [18]European Southern Observatory (ESO), Santiago, Chile. [19]Oukaimeden Observatory, High Energy Physics and Astrophysics Laboratory, Cadi Ayyad University, Marrakesh, Morocco. [20]Konkoly Observatory, Research Centre for Astronomy and Earth Sciences, Hungarian Academy of Sciences, Budapest, Hungary. [21]Instituto de Astrofísica de Andalucía (CSIC), Glorieta de la Astronomía, Granada, Spain. [22]Observatorio de Buenos Aires, Buenos Aires, Argentina. [23]Observatorio de Albox, Albox, Spain. *e-mail: pierre.vernazza@lam.fr

Supplementary material

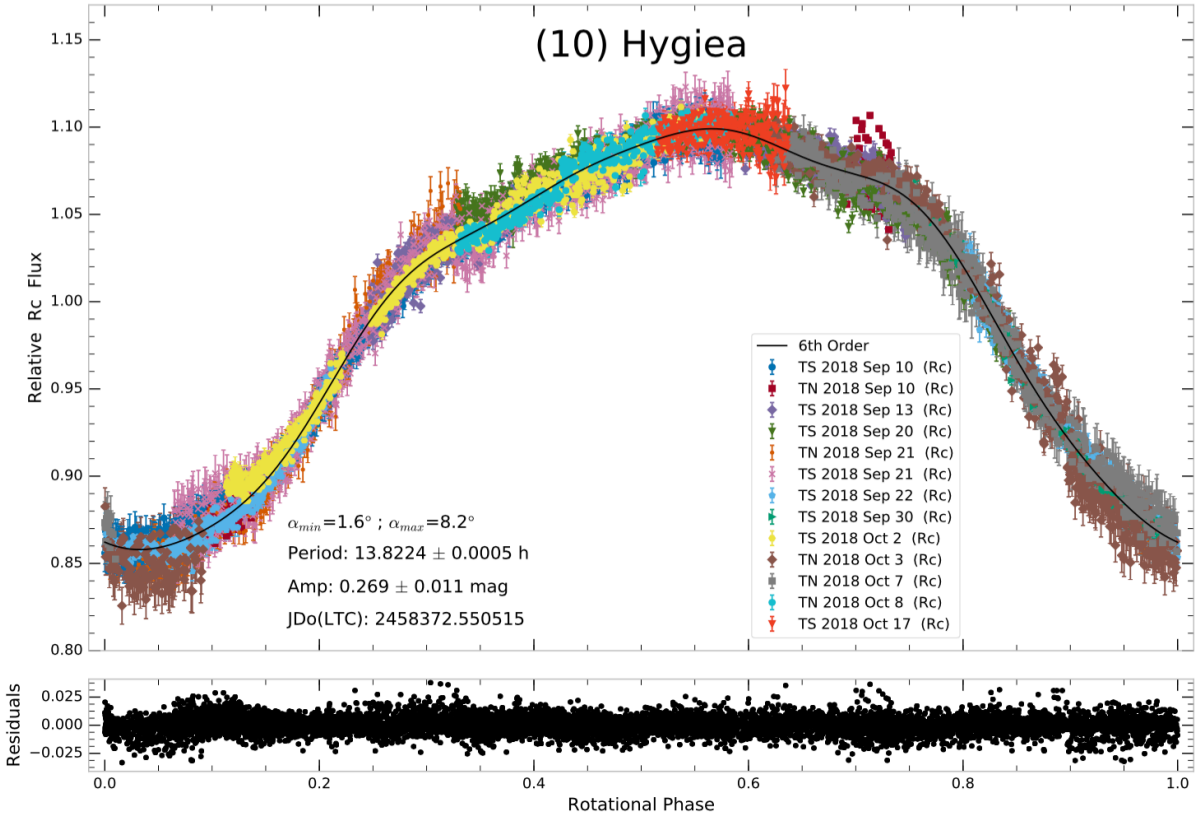

Supplementary Figure 1: New photometric observations of 10 Hygiea acquired with TRAPPIST N/S indicate a 13.8224h rotation period.

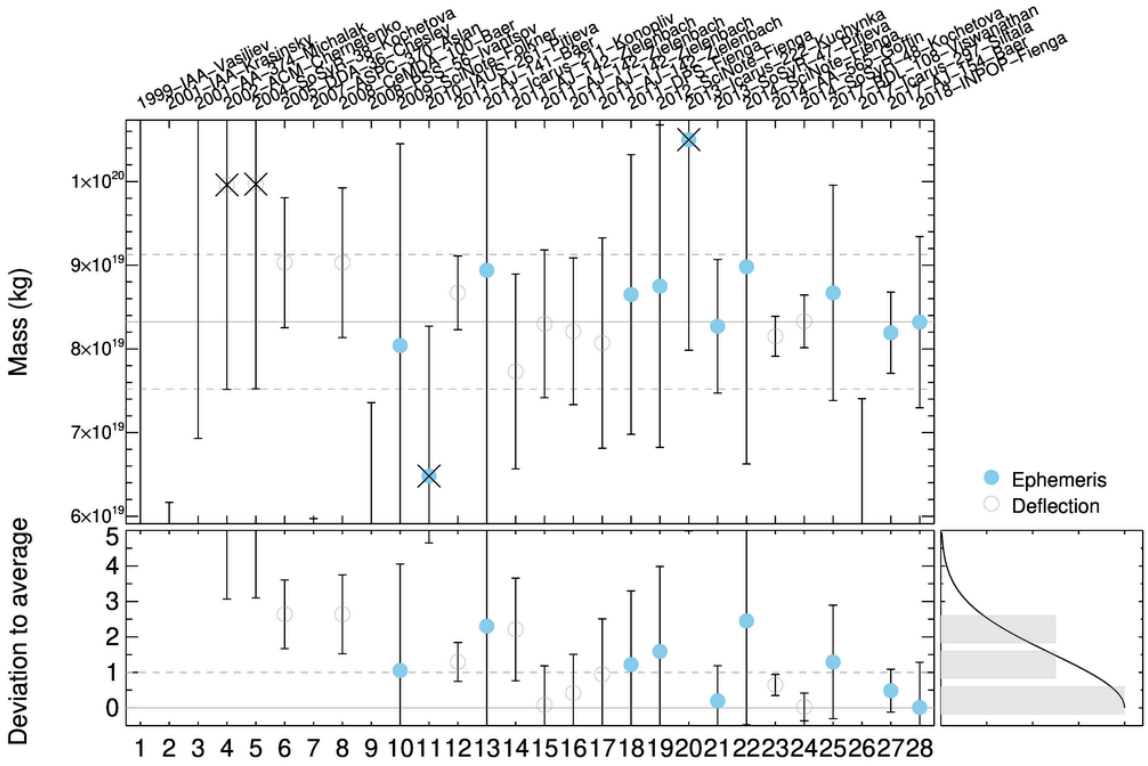

Supplementary Figure 2: Available mass estimates for Hygiea compiled from the literature. We evaluated the reliability of each value (see list in supplementary table 3) and estimated a representative value of $(8.32 \pm 0.80) \times 10^{19}$ kg following a well-proven procedure[52]. We used this value together with our new size estimate to compute Hygiea's bulk density of 1.94 ± 0.19 g cm^{-3}.

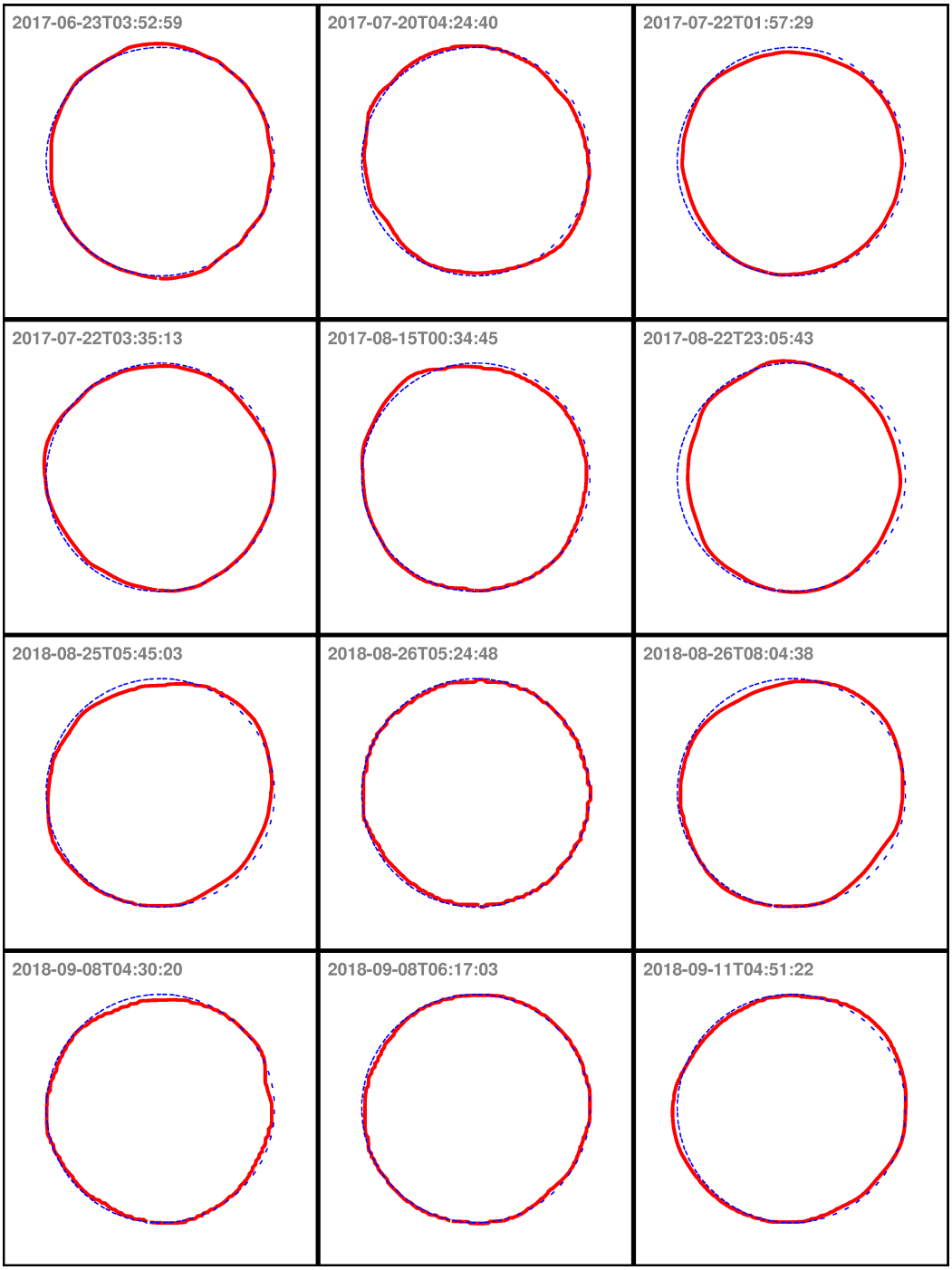

Supplementary Figure 3: Contour profiles of our Hygiea images (red) extracted for the 12 epochs compared to a mean radius sphere contour profile (blue). The size of the box for the x and y axes is 600 km. The precision of the VLT/SPHERE contour profiles is about 1 pixel (Fetick et al. 2019), that is typically ~5 km in the present case.

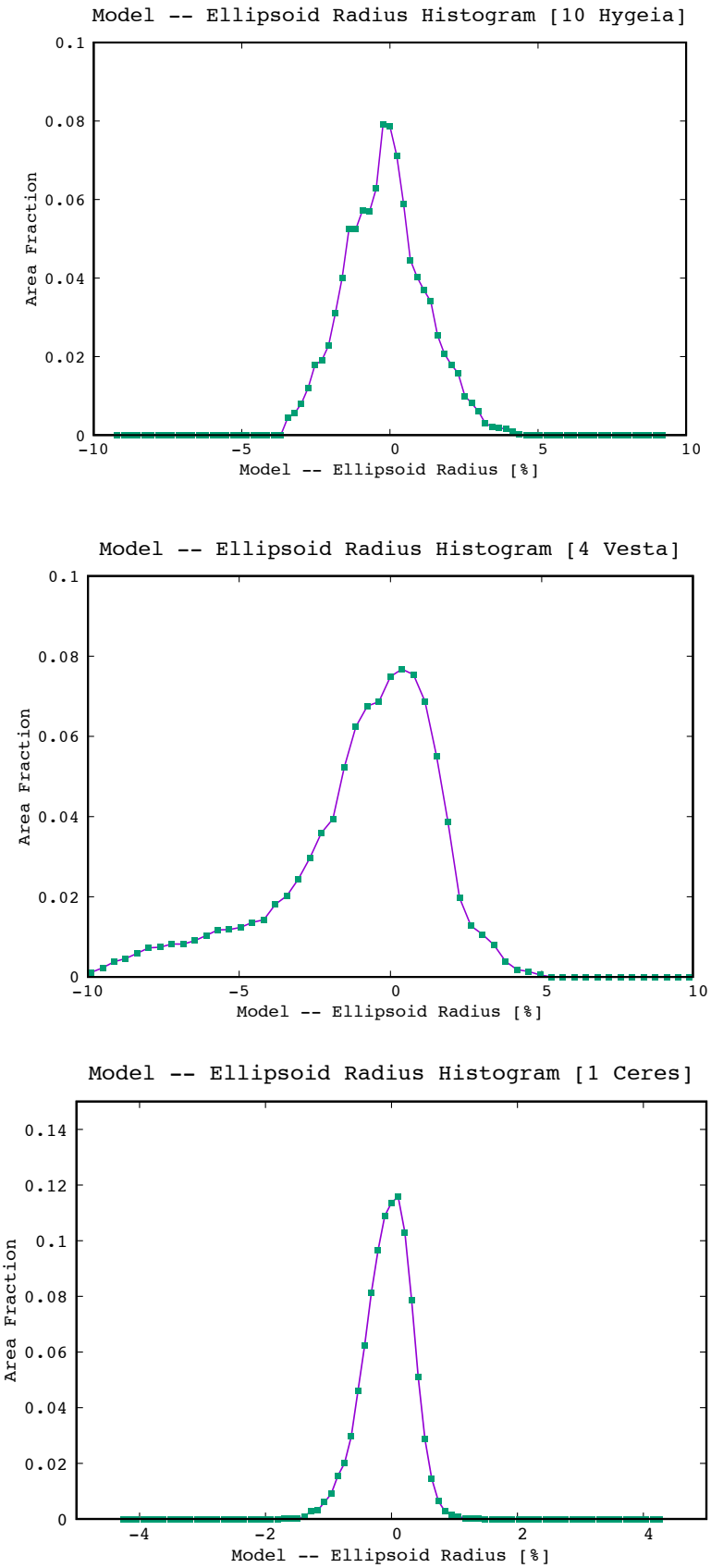

Supplementary Figure 4: Relative radial difference between the 3D shape models of (10) Hygiea, (4) Vesta and (1) Ceres and their best-fit ellipsoid. The differences have been

normalized by the average radius of the objects. These histograms highlight the absence of a large impact basin on both Hygiea and Ceres and the presence of a large depression on Vesta (large excess of 'negative' topography extending beyond -5% corresponding to -20km). The volume fraction of excavated material on Ceres, Vesta and Hygiea (calculted as |Volume_Body – Volume_Ellipsoid| / Volume _Body) is respectively 0.03%, 2% and 0.2%. In the case of Vesta, the surface of the basin was removed from the shape model prior to the fitting step. Such approach allowed a proper visualization of the surface topography.

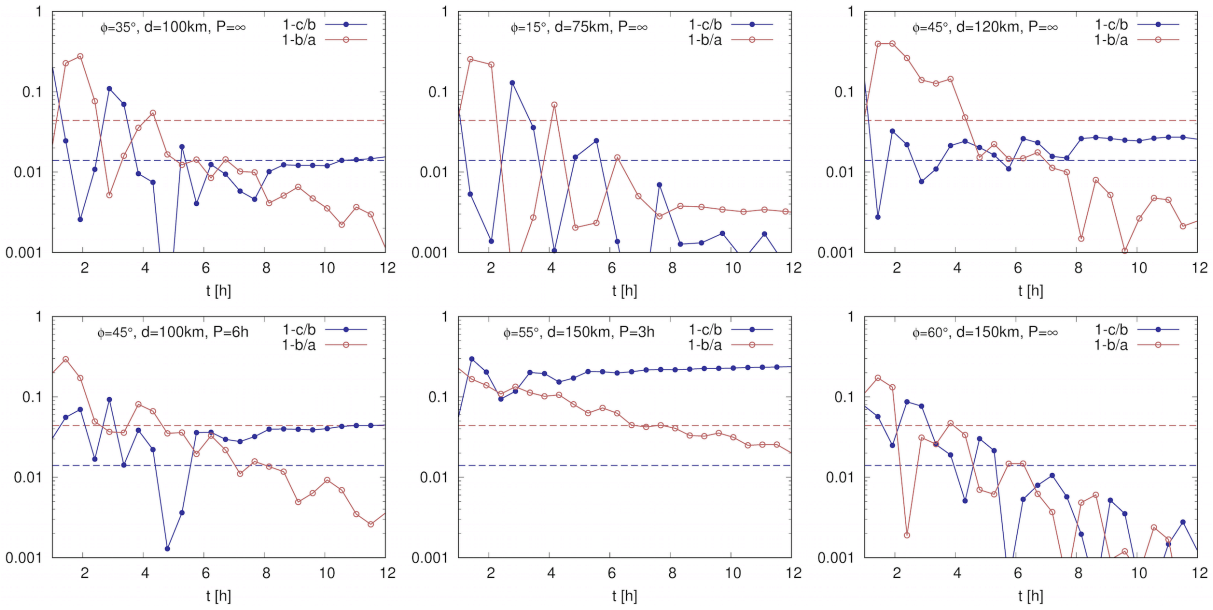

Supplementary Figure 5: Global oscillations for the largest remnant in our SPH simulations. Temporal evolution of the axis ratios 1-c/b (blue) and 1-b/a (red) is shown, along with the present-day observed values (dashed lines). In most simulations (5 out of 6), it is possible to find an agreement, typically around 4 ± 1 hours, which may be regarded as an estimate of the acoustic fluidization time span. When acoustic oscillations stop, the body suddenly regains its strength and the shape freezes. The impact angle, projectile size and initial rotation period are indicated on top.

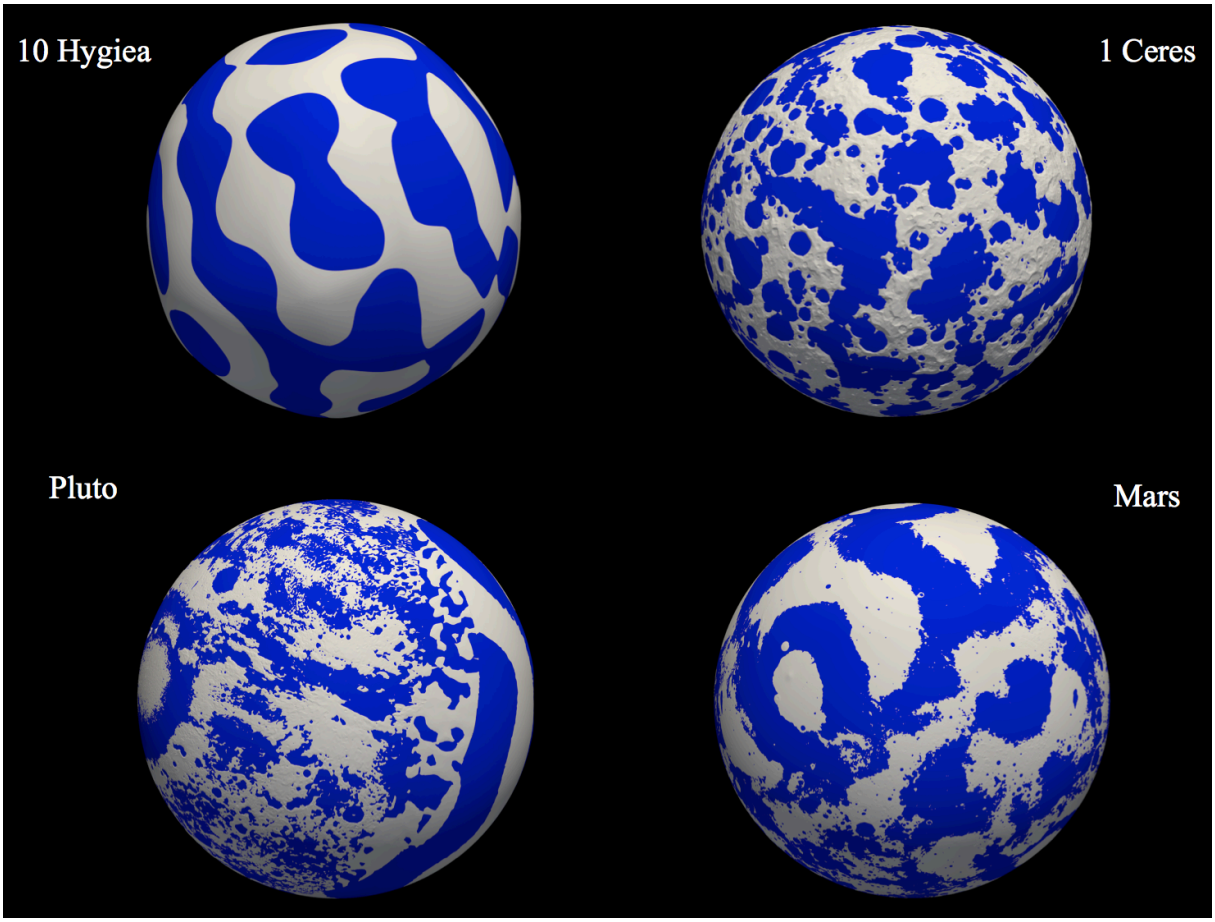

Supplementary Figure 6: Best-fit of the 3D shape models of Hygiea, Ceres, Pluto and Mars using the real spherical harmonic expansion coefficients. Here, we superimpose the 3D shape models of a few objects (gray) and the models derived from the spherical harmonics expansion (blue). The latter models were used to perform a proper calculation of the sphericity of all objects displyaed in Figure 4 (see main text) in order to avoid severe biases due to topography and/or different resolutions of the original 3D shape models.

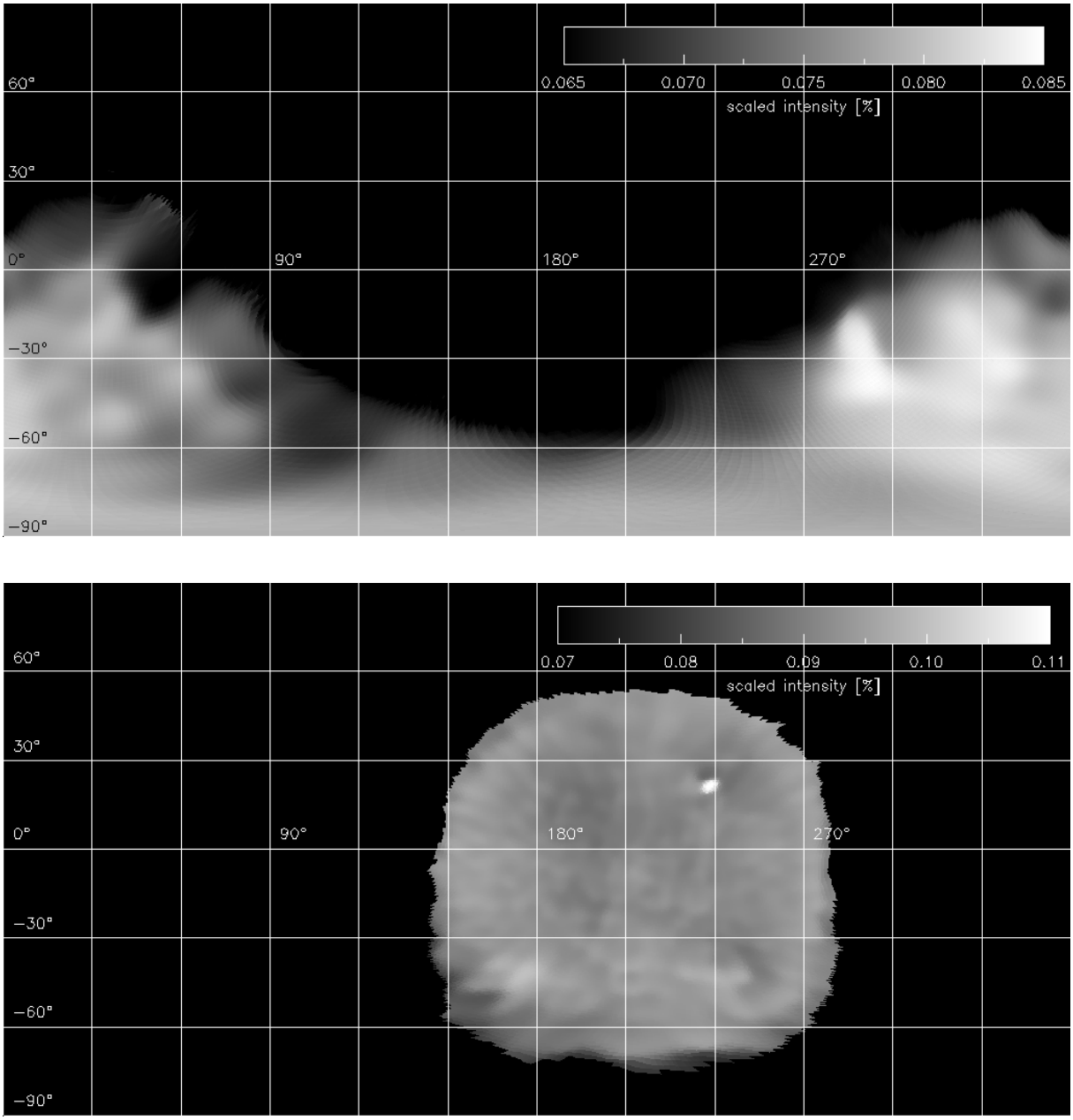

Supplementary Figure 7: Reflectance map of Hygiea (top) and Ceres (bottom) built from the best-quality images acquired with SPHERE for these objects, and scaled to their respective average geometric albedo.

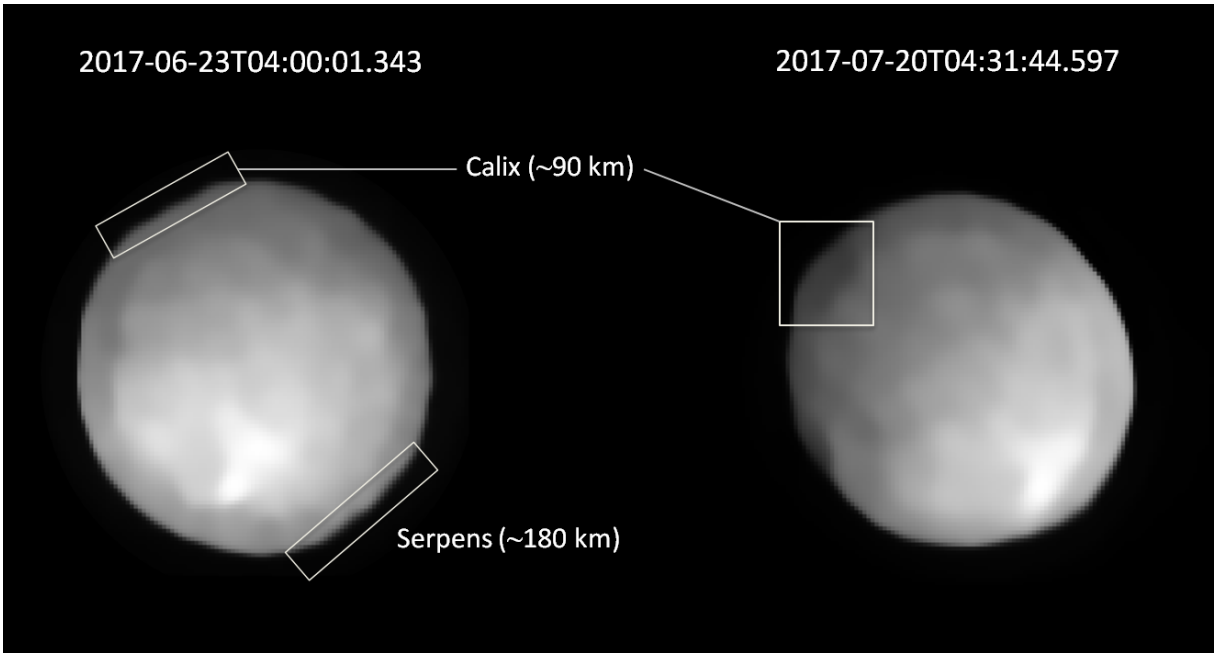

Supplementary Figure 8: Identification of the impact craters present at the surface of Hygiea. We identified 2 craters with respective diameters of 180 ± 15 km and 97 ± 10 km. The contours of the left image suggest that the two craters possess a central peak. Given that (10) Hygiea was named after the Greek goddess of health Hygieia, we used the related attributes of this divinity to name the two features. Specifically, Hygieia is always depicted holding a snake drinking from a cup, which lead us to name the two basins Serpens and Calix, a snake and a cup in latin respectively. Note that these two symbols (cup and snake) are widely used symbols in medicine and pharmacy.

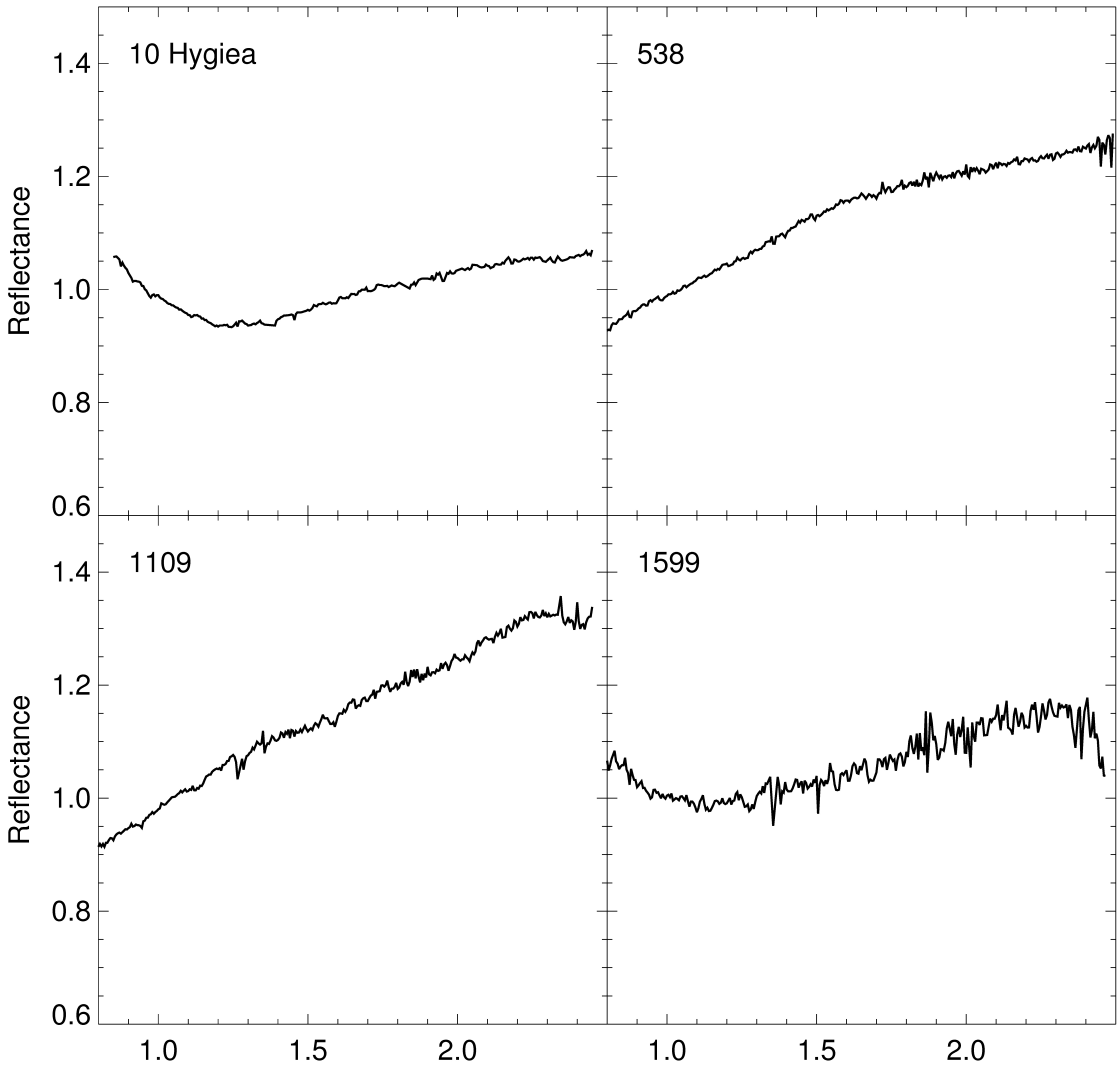

Supplementary Figure 9: Near-infrared reflectance spectra of Hygiea and possible family members. The spectra were collected with the NASA IRTF/Spex and normalized to unity at 1 micron. Both 538 Friederike and 1109 Tata are likely interlopers whereas 1599 Giomus's spectrum is compatible with the one of Hygiea suggesting a common origin for these two objects.

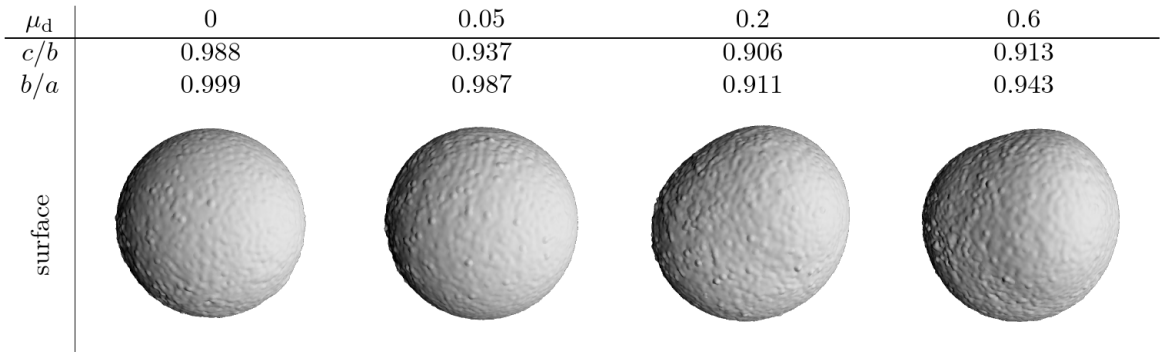

Supplementary Figure 10: Spherical shape requires very low friction coefficients. The shape of the largest remnant is shown for increasing values of the coefficient μ_d of dry friction. Columns show μ_d together with the resulting ratios of semi-axes c/b and b/a. To obtain a shape consistent with the observed one for (10) Hygiea, the friction coefficient needs to be as low as 0.1. This substantial weakening of the material can be attributed to acoustic fluidization.

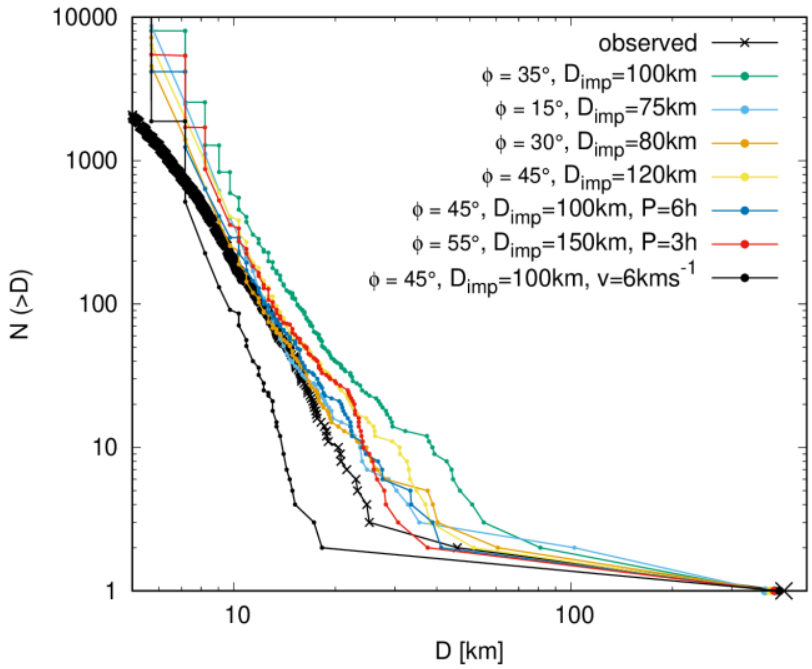

Supplementary Figure 11: Cumulative size-frequency distributions (SFD) of synthetic families, compared to the observed Hygiea family. The simulations are sorted from more energetic to less energetic, and the synthetic SFDs are slightly above or slightly below the observed one. Unless specified otherwise, the size of the target was D_{pb} = 428 km and the impact speed v_{imp} = 7 km/s. In the legend, φ denotes the impact angle and D_{imp} the size of impactor. For a certain range of impact parameters, intermediate-sized bodies are created by the impact. Here we compare the synthetic SFDs after the reaccumulation with the observed SFD; long-term collisional evolution and dynamical decay further decreasing $N(>D)$ is not yet taken into account.

Supplementary Table 1: Observational circumstances of our AO campaign. All observations were performed with the VLT/SPHERE/ZIMPOL instrument. For each observation, the table gives the epoch, the exposure time, the airmass, the distance to the Earth Δ and the Sun *r*, the phase angle α and the angular diameter D_a.

Date	UT	Exp (s)	Airmass	Δ (AU)	*r* (AU)	α (°)	D_a (’’)
2017-06-23	3:52:59	200	1.06	1.85	2.86	2.7	0.317
2017-06-23	3:56:30	200	1.05	1.85	2.86	2.7	0.317
2017-06-23	4:00:01	200	1.05	1.85	2.86	2.7	0.317
2017-06-23	4:03:31	200	1.04	1.85	2.86	2.7	0.317
2017-06-23	4:06:59	200	1.04	1.85	2.86	2.7	0.317
2017-07-20	4:24:40	200	1.05	1.92	2.88	8.0	0.305
2017-07-20	4:28:12	200	1.05	1.92	2.88	8.0	0.305
2017-07-20	4:31:44	200	1.06	1.92	2.88	8.0	0.305
2017-07-20	4:35:14	200	1.06	1.92	2.88	8.0	0.305
2017-07-20	4:38:44	200	1.07	1.92	2.88	8.0	0.305
2017-07-22	1:57:29	200	1.03	1.93	2.88	8.7	0.304
2017-07-22	2:01:01	200	1.03	1.93	2.88	8.7	0.304
2017-07-22	2:04:32	200	1.02	1.93	2.88	8.7	0.304
2017-07-22	2:08:02	200	1.02	1.93	2.88	8.7	0.304
2017-07-22	2:11:31	200	1.02	1.93	2.88	8.7	0.304
2017-07-22	3:35:13	200	1.01	1.93	2.88	8.7	0.304
2017-07-22	3:38:46	200	1.01	1.93	2.88	8.7	0.304
2017-07-22	3:42:16	200	1.02	1.93	2.88	8.7	0.304
2017-07-22	3:45:47	200	1.02	1.93	2.88	8.7	0.304
2017-07-22	3:49:17	200	1.02	1.93	2.88	8.7	0.304
2017-08-15	0:34:45	200	1.01	2.14	2.90	15.5	0.274
2017-08-15	0:38:17	200	1.01	2.14	2.90	15.5	0.274
2017-08-15	0:41:47	200	1.01	2.14	2.90	15.5	0.274
2017-08-15	0:45:18	200	1.01	2.14	2.90	15.5	0.274
2017-08-15	0:48:49	200	1.01	2.14	2.90	15.5	0.274
2017-08-22	3:05:43	200	1.08	2.24	2.91	17.1	0.262
2017-08-22	3:09:15	200	1.08	2.24	2.91	17.1	0.262
2017-08-22	3:12:46	200	1.07	2.24	2.91	17.1	0.262
2017-08-22	3:16:17	200	1.07	2.24	2.91	17.1	0.262
2017-08-22	3:19:47	200	1.06	2.24	2.91	17.1	0.262
2018-08-25	5:45:03	240	1.21	2.41	3.29	10.0	0.243
2018-08-25	5:49:13	240	1.21	2.41	3.29	10.0	0.243
2018-08-25	5:53:24	240	1.20	2.41	3.29	10.0	0.243
2018-08-25	5:57:34	240	1.20	2.41	3.29	10.0	0.243
2018-08-25	6:01:44	240	1.19	2.41	3.29	10.0	0.243
2018-08-26	5:24:48	240	1.24	2.40	3.29	9.7	0.244
2018-08-26	5:28:58	240	1.23	2.40	3.29	9.7	0.244

2018-08-26	5:33:08	240	1.22	2.40	3.29	9.7	0.244
2018-08-26	5:37:18	240	1.22	2.40	3.29	9.7	0.244
2018-08-26	5:41:28	240	1.21	2.40	3.29	9.7	0.244
2018-08-26	8:04:38	240	1.27	2.40	3.29	9.7	0.244
2018-08-26	8:08:49	240	1.28	2.40	3.29	9.7	0.244
2018-08-26	8:13:00	240	1.30	2.40	3.29	9.7	0.244
2018-08-26	8:21:17	240	1.32	2.40	3.29	9.7	0.244
2018-09-08	4:30:20	240	1.22	2.33	3.30	5.8	0.251
2018-09-08	4:34:31	240	1.21	2.33	3.30	5.8	0.251
2018-09-08	4:38:41	240	1.21	2.33	3.30	5.8	0.251
2018-09-08	4:42:51	240	1.20	2.33	3.30	5.8	0.251
2018-09-08	4:46:59	240	1.20	2.33	3.30	5.8	0.251
2018-09-08	6:17:03	240	1.19	2.33	3.30	5.7	0.251
2018-09-08	6:21:14	240	1.19	2.33	3.30	5.7	0.251
2018-09-08	6:25:23	240	1.19	2.33	3.30	5.7	0.251
2018-09-08	6:29:33	240	1.20	2.33	3.30	5.7	0.251
2018-09-08	6:33:42	240	1.21	2.33	3.30	5.7	0.251
2018-09-11	4:51:22	240	1.18	2.33	3.31	4.8	0.251
2018-09-11	4:55:31	240	1.17	2.33	3.31	4.8	0.251
2018-09-11	4:59:42	240	1.17	2.33	3.31	4.8	0.251
2018-09-11	5:03:52	240	1.17	2.33	3.31	4.8	0.251
2018-09-11	5:08:03	240	1.17	2.33	3.31	4.8	0.251

Supplementary Table 2: Observational circumstances of our lightcurve campaign with TRAPPIST (North and South). For each lightcurve, the table gives the epoch, the number of individual measurements N_p, Hygiea's distance to the Earth Δ and the Sun r, the phase angle α, the photometric filter and the telescope name.

Date	Np	Δ (AU)	r (AU)	α (°)	Filter	Site
2018-09-10	180	2.33	3.30	4.9	Rc	TRAPPIST-N
2018-09-10	1325	2.33	3.30	4.8	Rc	TRAPPIST-S
2018-09-13	698	2.32	3.31	3.8	Rc	TRAPPIST-S
2018-09-20	1215	2.31	3.31	1.9	Rc	TRAPPIST-S
2018-09-21	393	2.31	3.31	1.8	Rc	TRAPPIST-N
2018-09-21	1156	2.31	3.31	1.8	Rc	TRAPPIST-S
2018-09-22	975	2.32	3.32	1.6	Rc	TRAPPIST-S
2018-09-30	559	2.33	3.32	3.0	Rc	TRAPPIST-S
2018-10-02	990	2.34	3.32	3.6	Rc	TRAPPIST-S
2018-10-03	722	2.34	3.33	3.8	Rc	TRAPPIST-N
2018-10-07	568	2.36	3.33	5.1	Rc	TRAPPIST-N
2018-10-08	422	2.37	3.33	5.4	Rc	TRAPPIST-N
2018-10-17	287	2.43	3.34	8.2	Rc	TRAPPIST-S

Supplementary Table 3: Mass estimates of (10) Hygiea collected in the literature. For each, the 3σ uncertainty, method, selection flag, and bibliographic reference are reported. The methods are either deflection (DEFL) or ephemeris (EPHEM).

Mass ($\times 10^{19}$ kg)	Method	Selection	Reference
15.50 ± 14.91	DEFL	✗	53
5.57 ± 0.60	DEFL	✗	54
11.10 ± 4.17	DEFL	✗	55
9.96 ± 2.44	DEFL	✗	56
9.97 ± 2.45	DEFL	✗	57
9.03 ± 0.78	DEFL	✓	58
4.18 ± 1.79	EPHEM	✗	59
9.03 ± 0.89	DEFL	✓	60
4.97 ± 2.39	DEFL	✗	61
8.04 ± 2.41	EPHEM	✓	62
6.48 ± 1.79	EPHEM	✗	63
8.67 ± 0.44	DEFL	✓	64
8.94 ± 4.62	EPHEM	✓	65
7.73 ± 1.16	DEFL	✓	66
8.30 ± 0.88	DEFL	✓	66

8.21 ± 0.88	DEFL	✓	66
8.07 ± 1.26	DEFL	✓	66
8.65 ± 1.67	EPHEM	✓	67
8.75 ± 1.93	EPHEM	✓	68
10.50 ± 2.52	EPHEM	✗	69
8.27 ± 0.80	EPHEM	✓	69
8.98 ± 2.36	EPHEM	✓	70
8.15 ± 0.24	DEFL	✓	71
8.33 ± 0.31	DEFL	✓	72
8.67 ± 1.29	EPHEM	✓	73
4.93 ± 2.47	DEFL	✗	74
8.19 ± 0.49	EPHEM	✓	75
8.32 ± 1.02	EPHEM	✓	76
8.32 ± 0.80	**Average**		

Supplementary Table 4: Observational circumstances of our spectroscopic campaign. All near-infrared data were obtained using the IRTF/Spex instrument in low-resolution prism mode.

Asteroid	Date (UT)
10 Hygiea	28 Aug 2012
538 Friederike	03 Dec 2018
1109 Tata	20 Oct 2011
1599 Giomus	5 Sep 2010

Supplementary Table 5: Collision parameters of SPH simulations and parameters of the largest remnant. From left to right: diameter of the impactor, impact angle, impact speed, rotational period of the target, diameter of the largest remnant, rotation period of the largest remnant, ratio of semi-axes b and c of the largest remnant, ratio of semi-axes a and b. The last line of the table contains the parameters of (10) Hygiea. Although values of D_{lr} are systematically smaller than the size of Hygiea, we can rescale the simulation to match the value.

D_{imp} (km)	φ_{imp} (°)	V_{imp} (km/s)	P_{pb} (h)	D_{lr} (km)	P_{lr} (h)	c/b	b/a
100	45	6	6	416	73	0.999	0.999
100	45	7	6	403	9.5	0.944	0.999
120	45	7	∞	389	12.6	0.967	0.999
150	55	7	3	401	4.5	0.729	0.996
80	45	7	∞	420	138	0.999	0.999
80	30	7	∞	400	15.6	0.979	0.999
75	15	7	∞	378	19.7	0.987	0.999
100	35	7	∞	376	15.8	0.979	0.999
Observed (10) Hygiea				434	13.8	0.989	0.955

References

52. Carry, B. Density of Asteroids. *Planet. Space Sci.* **73**, 98 (2012).

53. Vasiliev, M. V. and Yagudina, E. I. Determination of masses for 26 selected minor planets from analysis of observations their mutual encounters with asteroids of lesser mass. Communications of IAA of RAS (1999).

54. Krasinsky, G. A., Pitjeva, E. V., Vasiliev, M. V., Yagudina, E. I. Estimating masses of asteroids. Communications of IAA of RAS (2001).

55. Michalak, G. Determination of asteroid masses. II. (6) Hebe, (10) Hygiea, (15) Eunomia, (52) Europa, (88) Thisbe, (444) Typtis, (511) Davida and (704) Interamnia. *A&A* **374**, 703-711, (2001).

56. Chernetenko, Y. A. and Kochetova, O. M. Masses of some large minor planets. Asteroids, Comets, and Meteors, 437-440 (2002).

57. Kochetova, O. M. Determination of Large Asteroid Masses by the Dynamical Method. *Solar System Research* **38**, 66-75 (2004).

58. Chesley, S. R., Owen, Jr., W. M., Hayne, E. W., Sullivan, A. M., Dumas, R. C., et al. The Mass of Asteroid 10 Hygiea. *Bulletin of the American Astronomical Society* **524** (2005).

59. Aslan, Z., Gumerov, R., Hudkova, L., Ivantsov, A., Khamitov, I., et al. Mass Determination of Small Solar System Bodies with Ground-based Observations. *Astronomical Society of the Pacific Conference Series* **370**, 52-58 (2007).

60. Baer, J. and Chesley, S. R. Astrometric masses of 21 asteroids, and an integrated asteroid ephemeris. *CMDA* **100**, 27-42 (2008).

61. Ivantsov, A. Asteroid mass determination at Nikolaev Observatory. *Planet. Space Sci.* **56**, 1857-1861 (2008).

62. Folkner, W. M. and Williams, J. G. and Boggs, D. H. The Planetary and Lunar Ephemeris DE 421. IPN Progress Report 42, 1-34 (2009).

63. Pitjeva, E. V. EPM ephemerides and relativity. *IAU Symposium* **26**, 170-178 (2010).

64. Baer, J. and Chesley, S. R. and Matson, R. D. Astrometric Masses of 26 Asteroids and Observations on Asteroid Porosity. *Astron. J.* **141**, 143-155 (2011).

65. Konopliv, A. S., Asmar, S. W., Folkner, W. M., Karatekin, O., Nunes, D. C., et al. Mars high resolution gravity fields from MRO, Mars seasonal gravity, and other dynamical parameters. *Icarus* **211**, 401-428 (2011).

66. Zielenbach, W. Mass Determination Studies of 104 Large Asteroids. *Astron. J.* **142**, 120-128 (2011).

67. Fienga, A., Kuchynka, P., Laskar, J., Manche, H. and Gastineau, M. Asteroid mass determinations with INPOP planetary ephemerides. EPSC-DPS Joint Meeting (2011).

68. Fienga, A., Manche, H., Laskar, J., Gastineau, M. and Verma, A. INPOP (2012).

69. Kuchynka, P. and Folkner, W. M. A new approach to determining asteroid masses from planetary range measurements. *Icarus* **222**, 243-253 (2013).

70. Fienga, A., Manche, H., Laskar, J., Gastineau, M. and Verma, A. INPOP (2014).

71. Goffin, E. Astrometric asteroid masses: a simultaneous determination. *A&A* **565** (2014).

72. Kochetova, O. M. and Chernetenko, Y. A. Mass determinations for 27 asteroids by the dynamic method. *Solar System Research* **48**, 295-301 (2014).

73. Viswanathan, V. and Fienga, A. and Gastineau, M. and Laskar, J. INPOP17a planetary ephemerides. *Notes Scientifiques et Techniques de l'Institut de mécanique celeste* **108** (2017).

74. Siltala, L. and Granvik, M. Asteroid mass estimation using Markov-chain Monte Carlo. *Icarus* **297**, 149-159 (2017).

75. Baer, J. and Chesley, S. R. Simultaneous Mass Determination for Gravitationally Coupled Asteroids. *Astron. J.* **154**, 76 (2017).

76. Fienga, A., et al.. *INPOP* (2018).